IEEE Access
Multidisciplinary | Rapid Review | Open Access Journal

Received November 21, 2021, accepted December 6, 2021, date of publication December 10, 2021,
date of current version December 24, 2021.

Digital Object Identifier 10.1109/ACCESS.2021.3134813

Modulation and Control of a DC-AC Converter With High-Frequency Link Transformer for Grid-Connected Applications

MAHMOUD A. SAYED[1], (Senior Member, IEEE), TAKAHARU TAKESHITA[2], (Senior Member, IEEE), ATIF IQBAL[3], (Senior Member, IEEE), ZUHAIR MUHAMMED ALAAS[4], (Member, IEEE), M. M. R. AHMED[5], (Member, IEEE), AND SHERIF M. DABOUR[6], (Senior Member, IEEE)

[1]Department of Electrical Power and Machines Engineering, Faculty of Engineering, South Valley University, Qena 83523, Egypt
[2]Department of Electrical and Mechanical Engineering, Nagoya Institute of Technology, Nagoya 466-8555, Japan
[3]Department of Electrical Engineering, Qatar University, Doha 2713, Qatar
[4]Electrical Engineering Department, Jazan University, Jazan 45142, Saudi Arabia
[5]Electrical Engineering Department, Faculty of Technology and Education, Helwan University, Cairo 11795, Egypt
[6]Department of Electrical Power Engineering, Faculty of Engineering, Tanta University, Tanta 31527, Egypt

Corresponding author: Mahmoud A. Sayed (mahmoud_sayed@ieee.org)

This publication was made possible by research collaboration between South Valley University, Nagoya Institute of Technology, Qatar University, and Jazan University. The statements made herein are solely the responsibility of the authors. The Open Access funding is provided by the South Valley University, Qena, Egypt.

ABSTRACT The need to integrate energy storage devices with renewable energy sources and improve the employed converters' modulation and control techniques continues to grow. This trend is further activated by utilizing new converter topologies, such as high-frequency (HF) link converters. A dc-ac with HF link isolated converter is presented in this paper to integrate a battery storage device with a three-phase grid. The proposed converter is composed of two stages. The first stage is a direct three-phase to single-phase bidirectional Matrix Converter (3×1 MC), which converts the standard three-phase voltages to a single-phase HF waveform. Besides, the MC ensures three-phase sinusoidal grid currents with a unity power factor (UPF). The second stage of the proposed topology is an H-Bridge Converter (HBC), which converts the battery dc-voltage to a single-phase HF waveform synchronized with that of the single-phase output of the MC. Therefore, HF terminals of both stages have been linked by a single-phase HF transformer that provides galvanic isolation to the system. Also, a new mathematical model has been presented to obtain the accurate duty cycles of all matrix converter switches. Moreover, a new Pulse Width Modulation (PWM) technique of the analyzed converter with the controllable voltage limits is introduced. A simple control method is presented to regulate the battery dc-current and match reference value using a single PI controller. A laboratory prototype-based 200V, 2kW has been carried out to investigate the proposed technique's validity.

INDEX TERMS DC-AC-AC converter, isolated grid-connected converter, matrix converter, PWM.

I. INTRODUCTION

In the past two decades, the global warming phenomenon has been the most significant threat facing the planet. Accordingly, there was an international consensus to countermeasure global warming and compensate for the lack of electrical power generation by increasing the penetration of Renewable Energy Sources (RES) [1], [2]. Furthermore, due to the dependence of the generated power from RES on the weather changes, Energy Storage Systems such as batteries should be integrated into these systems to configure the microgrids (MGs) [3].

The Battery Storage System (BSS) manages the power mismatch between load/grid power demanded and RES at the load variation. It also improves the power quality and reliability of the main grid [4]–[6]. Thus, dc-ac bidirectional converters should be used to interface between BSS and the grid to manage the bidirectional power flow during the charging and discharging process [7]. Bidirectional dc-ac converters in grid-tied applications include galvanic isolation

The associate editor coordinating the review of this manuscript and approving it for publication was Tao Wang.

between the ac and dc sides and are recommended in the standards grid-connected systems (e.g., German codes VDE 0126-1-1) to avoid the leakage current and for safety issues.

This paper focuses on a dc-ac converter for a BSS, representing the key component for integrating the microgrids with a RES. From the past efforts, the galvanic isolation in BSS is commonly introduced in two ways [7]: (a) using standard line-frequency transformers (LFT) at the grid side, and (b) utilizing medium or high-frequency transformers (HFT) that link an intermediate ac stage in the system [8]–[11].

Although the single-stage grid-tied dc-ac converter with LFT has a simple structure and ensures sinusoidal grid currents with a unity power factor (UPF), the HFT based converters offer a smaller footprint, and less copper wire, hence reducing overall system losses and enhancing efficiency with a lower cost [7]. This, among other features, increases the attention towards the HFT based converter, which can be employed in different topologies and applications [8]–[31]. A comprehensive review of HFT-based converter topologies, corresponding controller, associated application, and implementation problems was introduced in [8]. Three-port HFT-based converters to integrate three isolated circuits were discussed in [9], [10]. The intermediate HFT-based dc-ac converters are commonly considered [11]–[16]. It has two basic architectures, as shown in Fig. 1. The conventional type is shown in Fig. 1(a) [11]–[13]. It uses a back-to-back (B2B) converter in the grid-side to achieve an ac HF voltage waveform at the terminal of HFT and uses an ac-dc voltage source converter (VSC) on the battery side. It is important to note that this configuration provides acceptable dynamic performance and injects sinusoidal grid currents with low Total Harmonic Distortion (THD) [12]. However, this architecture utilizes a bulky dc-link capacitor, which has low resistance to environmental conditions and reduces the overall system's reliability. Moreover, it increases the number of stages and therefore increases the system cost, footprint, overall power losses and reduces the system efficiency and lifetime [14]. Alternatively, the architecture of Fig. 1(b) uses a direct three-by-single-phase bidirectional matrix converter (3×1 MC), in which no dc-link capacitor is utilized, as can be seen in Fig. 1(b). The MC gives the system a longer lifespan, reduces the system stages, volume, and size. In addition, the use of the MC improves the system dynamic characteristics [14]–[18].

As a research hotspot combining the features of MC topology into the dc-ac grid-connected converters, this combination with LFT has been dramatically explored from various aspects [19]–[24]. In [19]–[22], a three-phase MC was presented as a single-stage grid-tied dc-ac bidirectional converter for BSS with LFT. Although this system ensures sinusoidal grid current with a UPF, the galvanic isolation is employed at the grid side with a conventional three-phase LFT. Moreover, an isolated ac-ac-dc converter considering unidirectional power flow was presented in [23]. Also, bidirectional power flow of the ac-ac-dc converter considering dc load voltage regulation and sinusoidal three-phase grid current was presented in [24]. However, all switches of

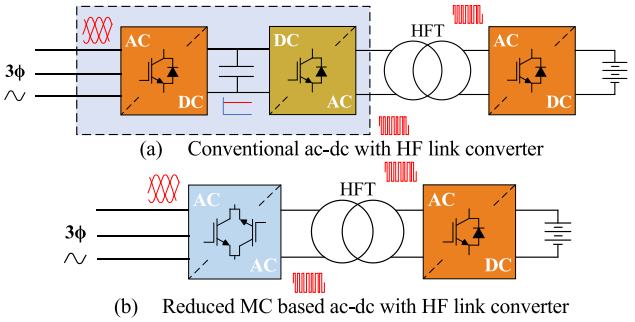

FIGURE 1. The schematic diagram for ac-dc with HF link converters.

HBC in these topologies at the dc side were represented by common- collector bidirectional switches.

Alternatively, the HFT based configurations of Fig. 1 have been extensively explored in the literature for various applications, such as BSS [12]–[16] and wind energy conversion systems (WECS) [17], [18], [18], [25], [26].

More advantages of utilizing both architectures for WECS are raised; the galvanic isolation provided by the medium and HFTs moves the insulation problem from the generator-side to the transformer secondary-side, which leads to the use of a passive rectifier for the ac–dc conversion [18]. Moreover, it enables the dc series and ac parallel connection of the wind farms to extensively reduce the system losses and costs and increase the reliability [25], [26]. It is worth mentioning that the combination of medium or HF-link with MC topology, investigated in [17], [18] for offshore wind farms, increases the system efficiency. In addition, it introduces a flexible topology for this application, whereas it enables different types of operation with a simpler structure compared with conventional approaches. Moreover, advanced PWM techniques for the same topology were proposed in [14], [16] for accurate UPF.

The combination of reduced MC with HFT in the converter topology was presented in [17] for offshore wind farm application and considered in [14]–[16] for the grid-connected systems. The same topology is used in this paper for a BSS, in which the battery terminals replace the HVDC transmission system terminals. Unfortunately, the presented PWM switching techniques in [14], [15] result in grid currents problems, in which the three-phase grid currents have a THD of more than 10%, which exceeds the IEEE standard's grid permissible limits. From the understanding gained, few studies have focused on the grid current problems. A modified mathematical model of the MC to reduce grid current harmonic components is proposed [16]. Another approach has been shown in [27] to reduce the grid current harmonics based on the space vector PWM technique. However, these solutions are complex in implementation, and therefore the related research work on the modulation and control techniques of this topology for the grid-connected applications, especially those used to integrate RES and BES systems, still needs improvements. Moreover, different control schemes are introduced to control the ac-dc converters operations and

improve the active and reactive power flow are presented in [28]–[30].

On the other hand, the soft-switching techniques represent one of the main critical aspects that should be considered for the HFT-based converters to reduce the size of the passive component and the switching losses [31]. It is mainly classified into 1) passive, 2) active, and 3) natural soft-switching techniques. The passive technique is considered in [15] for the HFT-based grid-tie dc–ac converters by connecting shunt ceramic snubber capacitor across each active switch. Although the snubber capacitors increase the system efficiency in high power applications due to the high current that can exchange stored energy between snubber capacitors across the OFF-going and ON-coming switches during the dead-time, it reduces the efficiency at low power applications due to the circulating current between snubber capacitors and switches [15]. The active soft switching incorporates additional switches, which are turned ON at a preset time before turning ON the main switch [28]. However, this solution increases the system size, cost, and complexity. In this paper, a natural soft switching is performed for the HBC based on the switching technique of both MC and HBC without using additional components and depending only on the commutation charge of the parasitic switch capacitance and the time of commutation current.

Given the many benefits of the strategy of Fig. 1(b) and motivated by the technical challenges, this paper now aims to introduce a new simple and more sophisticated modulation and control technique to solve the problems mentioned above. This PWM modulation technique's key contribution is to provide a simple approach to ensure a real power injection at UPF to the grid from a dc battery in the proposed system. Furthermore, it is also used to inject a sinusoidal current to the MC output voltage, allowing bidirectional flow.

In summary, the merits of using the analyzed topology with the proposed modulation and control technique can be listed as follows:

1) The analyzed configuration provides galvanic isolation by utilizing HF transformers (HFT).
2) The absence of the dc-link capacitor in the MC gives the systems a longer lifespan, reduces the system stages, and improves their dynamic characteristics.

Moreover, the novelty and key contributions that are carried out from this paper can be written as follows:

1) A new mathematical model of the system with accurate duty cycles of all matrix converter bidirectional switches is proposed.
2) A new straightforward PWM switching technique is proposed to achieve the maximum allowable VTR.
3) The proposed switching technique achieves natural soft switching for the H-bridge circuit. It also obtains sinusoidal grid currents with UPF and low THD according to the IEC-61000-standard.
4) Moreover, a simple control technique to regulate the battery current is presented using one PI controller.

Alongside the above merits, it can be mentioned that the proposed system has the following features

1) a small footprint, low cost, and higher efficiency,
2) simple modulation and control techniques,
3) sinusoidal grid current with UPF, and
4) high efficiency (about 93% as in the case study).

These features make the proposed switching technique for the system under study particularly valuable in integrating the BSS with RES in the future power grid.

The rest of this paper is classified as follows: section II introduces the proposed grid-connected dc-ac converter's operation. Then, the system configuration is modeled and analyzed in section III. A new switching pattern for the MC is introduced in section IV, including the duty cycle and controllable range derivations. Section V presents the PWM switching pattern of the HBC. The system control technique is introduced in section VI. Finally, a laboratory prototype-based 200V and 2kW has been carried out in section VII to validate and verify the proposed system and its control technique.

II. THE GRID-CONNECTED ISOLATED DC-AC CONVERTER

The power circuit topology of the proposed dc-ac-ac grid-connected converter is shown in Fig. 2. The converter consists of two stages connected through an HFT. The first stage is direct 3×1 MC, while the second one is a conventional HBC. The HBC has four switches S_{jp} to S_{kn}. Whereas the direct 3×1 MC has six four-quadrant switches S_{ug} to S_{wh}. The MC is used to perform the following operations: a) convert the standard three-phase grid voltage to an HF single-phase voltage waveform, and b) ensure sinusoidal grid current waveform with UPF. Whereas the HBC converts the dc voltage of the battery to a high-frequency single-phase voltage waveform, which should be synchronized with MC single-phase output. Therefore, single-phase HFT with a unity turns ratio links HBC and MC to accommodate both sides' galvanic isolation.

The MC is connected to the grid through an ac-filter to eliminate the grid current harmonics and ensure sinusoidal current waveforms. Practically, near sinusoidal currents are achieved with an acceptable THD level with a minimal effect on the power factor, which can be compensated using the control algorithm to obtain an accurate UPF at the grid side. The detailed design procedure of the ac-filter was presented in [16]. It is important to note that SiC-MOSFETs have been used as the power switches for HBC and MC to provide high-frequency switching at low power loss.

III. MODELING OF THE ISOLATED AC-AC-DC CONVERTER

The effect of the ac-filter at the grid side of MC can be ignored to simplify the analysis. Therefore, the grid phase voltages (e_{su}, e_{sv}, e_{sw}) and line voltages (e_{suv}, e_{svw}, e_{swu}) are defined as follows:

$$\begin{bmatrix} e_{su} \\ e_{sv} \\ e_{sw} \end{bmatrix} = \sqrt{\frac{2}{3}}E \begin{bmatrix} \cos(\theta) \\ \cos\left(\theta - 2\pi/3\right) \\ \cos\left(\theta + 2\pi/3\right) \end{bmatrix} \quad (1)$$

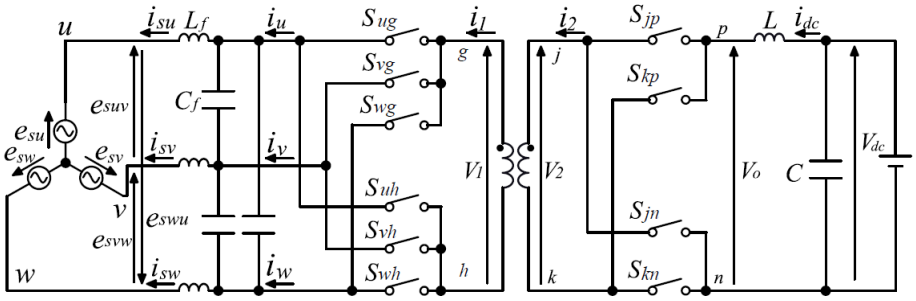

FIGURE 2. The topology of the grid-connected DC-AC-AC converter.

$$\begin{bmatrix} e_{suv} \\ e_{svw} \\ e_{swu} \end{bmatrix} = \begin{bmatrix} e_{su} - e_{sv} \\ e_{sv} - e_{sw} \\ e_{sw} - e_{su} \end{bmatrix} = \sqrt{2}E \begin{bmatrix} \cos(\theta + \pi/6) \\ \cos(\theta - \pi/2) \\ \cos(\theta + 7\pi/6) \end{bmatrix} \quad (2)$$

where E is the line voltage effective value and θ is the displacement angle between the voltage and current of the grid, which can be determined by the line angular frequency ω and an arbitrary angle φ^* as follows:

$$\theta = \omega t + \varphi^* \quad (3)$$

The reference three-phase current of the MC (i_u^*, i_v^*, and i_w^*) can be formulated as given in (4)

$$\begin{bmatrix} i_u^* \\ i_v^* \\ i_w^* \end{bmatrix} = \sqrt{2}I^* \begin{bmatrix} \cos(\theta + \varphi^*) \\ \cos(\theta - 2\pi/3 + \varphi^*) \\ \cos(\theta + 2\pi/3 + \varphi^*) \end{bmatrix} \quad (4)$$

where I^* is the reference current magnitude of the grid.

Based on the power invariant concept and by considering lossless MC, the reference current magnitude can be determined as follows:

$$v_1 i_1 = e_\alpha i_u^* + e_\beta i_v^* + e_\gamma i_w^* = \sqrt{3}EI^* \cos\varphi^* \quad (5)$$

Therefore, the reference grid current is governed by

$$I^* = \begin{cases} \dfrac{v_1 i_1}{\sqrt{2}\left(e_\alpha \cos\vartheta_\alpha + e_\beta \cos\vartheta_\beta + e_\gamma \cos\vartheta_\gamma\right)} \\ \dfrac{v_1 i_1}{\sqrt{3}E\cos\varphi^*} \end{cases} \quad (6)$$

where

$$\begin{cases} \vartheta_\alpha = \theta + \varphi^* \\ \vartheta_\beta = \theta + \varphi^* - 2\pi/3 \\ \vartheta_\gamma = \theta + \varphi^* + 2\pi/3 \end{cases}$$

The MC duty cycles, $d_{ug} - d_{wh}$ should be decided according to the reference single-phase HF voltage and the reference grid current. On the other hand, duty cycles of the HBC, $d_{jp} - d_{kn}$ should be decided according to the reference single-phase HF voltage and the reference dc current.

IV. PROPOSED SWITCHING PATTERNS OF THE MC

Fig. 3 shows the MC analytical model. In this model, the three-phase grid voltages are represented by e_α, e_β, and e_γ according to their levels, which are the maximum, middle and minimum, respectively. Therefore, $e_\alpha > e_\beta > e_\gamma$. The same definition can be applied to the grid currents $i_\alpha > i_\beta > i_\gamma$.

The proposed switching pattern is designed based on switching the positive input terminal with the maximum and middle grid terminals α, β, whereas the negative input terminal is switched only with the middle and minimum grid terminals β, γ. Fig. 4 shows the current direction and the active switches during the positive and negative half cycles of the MC input voltage v_1. It can be observed that in the positive half-cycle shown in Fig. 4(a), the positive terminal g is switched only with the grid terminals α and β to realize positive average voltage during a control period of T_s, while the negative terminal h is switched only with the grid terminals β and γ to realize negative average voltage during another T_s. In the negative half-cycle shown in Fig. 4(b), the negative terminal g is switched only with the grid terminals β and γ, whereas the positive terminal h is switched only with the grid terminals α and β.

Fig. 5 shows the proposed switching strategy, the grid injected current waveforms and the high-frequency input voltage of the MC. The suggested switching pattern is defined during the period of $0 < \theta < \pi/3$ when the input voltage $e_{su} > e_{sv} > 0 > e_{sw}$. Therefore, the three-phase voltages e_{su}, e_{sv}, e_{sw} are represented by $e_\alpha, e_\beta, e_\gamma$, respectively. The switching pattern enables the current to flow in

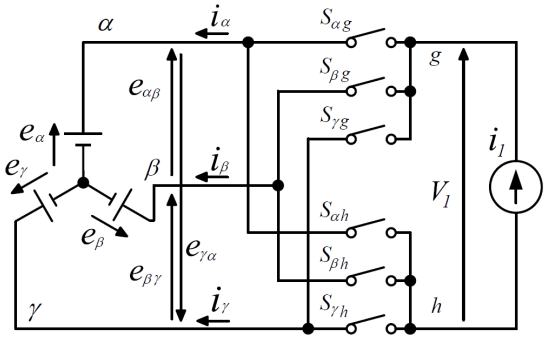

FIGURE 3. The direct 3X MC Equivalent circuit.

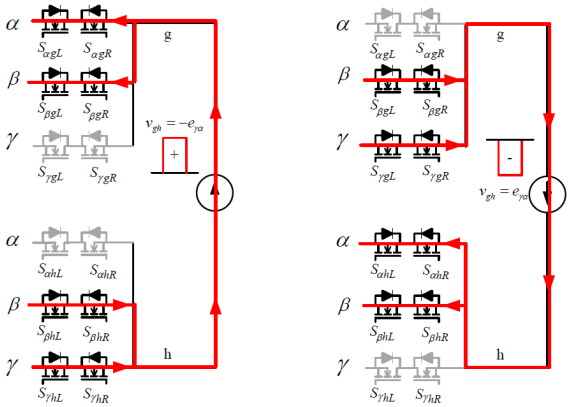

(a) during positive half-cycle (b) during negative half-cycle

FIGURE 4. Current directions in the direct 3 × 1 MC.

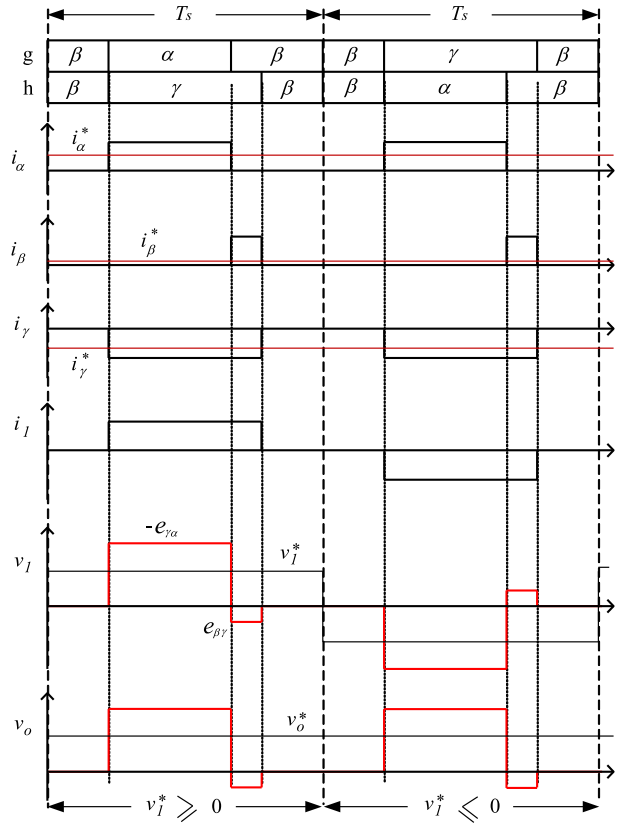

FIGURE 5. Proposed switching pattern of the direct 3 × 1 MC.

both directions. During their period of $2T_s$, the high-frequency single-phase voltage and current waveforms V_1, I_1 of the MC are in-phase.

A. DUTY CYCLES OF THE 3 × 1 MC

The constraints of all switches duty cycles for the MC can be formulated as:

$$\begin{cases} d_{ug} + d_{vg} + d_{wg} = 1 \\ d_{uh} + d_{vh} + d_{wh} = 1 \end{cases} \tag{7}$$

According to the PWM pattern shown in Fig. 5, the reference three-phase injected currents to the grid by the direct 3×1 MC $i_\alpha^*, i_\beta^*, i_\gamma^*$ can be formulated as follows:

$$\begin{cases} i_\alpha^* = (d_{\alpha g} - d_{\alpha h})\, i_1 \\ i_\beta^* = (d_{\beta g} - d_{\beta h})\, i_1 \\ i_\gamma^* = (d_{\gamma g} - d_{\gamma h})\, i_1 \end{cases} \tag{8}$$

The grid injected power p_g can be formulated as follows.

$$P_g = e_\alpha i_\alpha^* + e_\beta i_\beta^* + e_\gamma i_\gamma^* = \sqrt{3} E I^* \cos\varphi^* \tag{9}$$

Assuming a lossless power conversion, the grid injected power can be formulated as follows.

$$P_g = v_1^* i_1 \tag{10}$$

Based on equations (9) and (10), the current I^* can be formulated as follows.

$$I^* = \frac{v_1^* i_1}{\sqrt{3} E \cos\varphi^*} \tag{11}$$

During the positive half-cycle of the voltage of MC, $v_1^* > 0$, the terminal g is switched only with the grid high current phases α and β, while the terminal h is switched only with the grid low current phases β and γ. Therefore, the switches $S_{\gamma g}$ and $S_{\alpha h}$ are off during this switching period T_s and their duty cycles are zero. According to (8), all switches of the MC can be controlled using the following duty cycles:

$$\begin{cases} d_{\alpha g} = \dfrac{i_\alpha^*}{i_1}, \quad d_{\beta g} = 1 - \dfrac{i_\alpha^*}{i_1}, \quad d_{\gamma g} = 0 \\ d_{\alpha h} = 0, \quad d_{\beta h} = 1 + \dfrac{i_\gamma^*}{i_1}, \quad d_{\gamma h} = -\dfrac{i_\gamma^*}{i_1} \end{cases} \tag{12}$$

Furthermore, during the negative half-cycle, $v_1^* < 0$, the switching pattern is reversed. The terminal g is switched only with the low current grid phases β and γ, while the terminal h is switched only with the high current grid phases α and β. The switches $S_{\alpha g}$ and $S_{\gamma h}$ are off during this switching period T_s and their duty cycles are zero. Therefore, the duty cycles of all MC switches, in this case, can be formulated as follows:

$$\begin{cases} d_{\alpha g} = 0, \quad d_{\beta g} = 1 - \dfrac{i_\gamma^*}{i_1}, \quad d_{\gamma g} = \dfrac{i_\gamma^*}{i_1} \\ d_{\alpha h} = -\dfrac{i_\alpha^*}{i_1}, \quad d_{\beta h} = 1 + \dfrac{i_\alpha^*}{i_1}, \quad d_{\gamma h} = 0 \end{cases} \tag{13}$$

B. RANGE OF CONTROL

In general, the 3×1 MC duty cycles should be within limits {0-1} to avoid the overmodulation operating region. Therefore, VTR's constraints and the reference power factor angle must be determined according to the duty cycle limits. The controllable limits are the same in the case of $v_1 > 0$ and $v_1 < 0$. Considering the time of $0 \leq \theta \leq \pi/3$, the controllable limit can be determined based on the duty cycles $i_\alpha^*/I_1 (= d_{\alpha g})$, $-i_\gamma^*/I_1 (= d_{\gamma h})$ shown in (12) and (13), as follows;

$$\begin{cases} 0 \leq \dfrac{i_\alpha^*}{I_1} = \dfrac{\sqrt{2} V_1^* cos\,(\theta + \varphi^*)}{\sqrt{3} E\, cos\varphi^*} \leq 1 \\ 0 \leq \dfrac{i_\gamma^*}{I_1} = -\dfrac{\sqrt{2} V_1^* cos\,(\theta + \varphi^* + 2\pi/3)}{\sqrt{3} E\, cos\varphi^*} \leq 1 \end{cases} \tag{14}$$

1) CONTROLLABLE RANGES OF POWER FACTOR ANGLE

According to (14), a positive duty cycle can be achieved based on the power factor reference angle φ^*. Furthermore, the grid phase angle θ, as follows.

$$\begin{cases} \dfrac{cos\,(\theta+\varphi^*)}{cos\varphi^*} \geq 0 \\ -\dfrac{cos\,(\theta+\varphi^*+2\pi/3)}{cos\varphi^*} \geq 0 \end{cases} \tag{15}$$

Thus, the ranges of controlling the input current phase angle are obtained from (15) can be governed by (16) as follows:

$$\begin{cases} -\dfrac{\pi}{6} \leq \varphi^* \leq \dfrac{\pi}{6} \\ \dfrac{5\pi}{6} \leq \varphi^* \leq \dfrac{7\pi}{6} \end{cases} \tag{16}$$

2) CONTROLLABLE RANGES OF THE OUTPUT VOLTAGE MAGNITUDE

According to (16), the relation between the input and grid voltages of the matrix converter can be formulated as follows;

$$\begin{cases} \dfrac{\sqrt{2}V_1^*\cos\,(\theta+\varphi^*)}{\sqrt{3}E\cos\varphi^*} \leq 1 \\ -\dfrac{\sqrt{2}V_1^*\cos\,(\theta+\varphi^*+2\pi/3)}{\sqrt{3}E\cos\varphi^*} \leq 1 \end{cases} \tag{17}$$

Therefore, the controllable ranges of the MC voltage are obtained from (19) as follows:

$$-\sqrt{6}\Big/2E\cos\varphi^* \leq V_1^* \leq \sqrt{6}\Big/2E\cos\varphi^* \tag{18}$$

V. SWITCHING PATTERN OF THE HBC

Fig. 6 shows the analytical model of the HBC. It converts the battery dc voltage and current to a high-frequency signal transferred to the MC through the HFT. Since the HFT turns ratio is one, the input and output voltages V_1, V_2 are ideally the identical waveforms. Therefore, the switching pattern depends mainly on the output voltage of the HBC, V_2.

Fig. 7 shows the switching signals and input and output voltages waveforms, V_o, V_1 of the HBC. As can be observed, the PWM switching pattern of the HBC has been divided into four operation modes: $M1$ to $M4$. The equivalent circuits and the current directions of the HBC during the modes are shown in Fig. 8. It is clear to see that the current direction of the battery side is the same, whereas the current direction of the HF-side is alternative according to the voltage waveform V_2.

VI. NATURAL SOFT-SWITCHING TECHNIQUE

In this paper, the operation of the H-bridge circuit provides natural soft-switching without using any additional components, as can be observed from Fig. 6. In the case of battery charging, the power flow from the MC side (primary side) to the HBC side (secondary side). Therefore, the current is flowing in the body diode of the upper and lower switches of the H-bridge. In the battery discharging case, the switching actions of the HBC have been realized according to the switching pattern shown in Fig. (7), in which four modes of

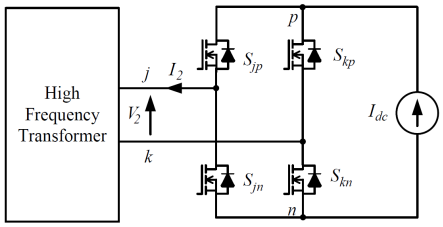

FIGURE 6. Equivalent circuit of the DC-AC H-bridge converter.

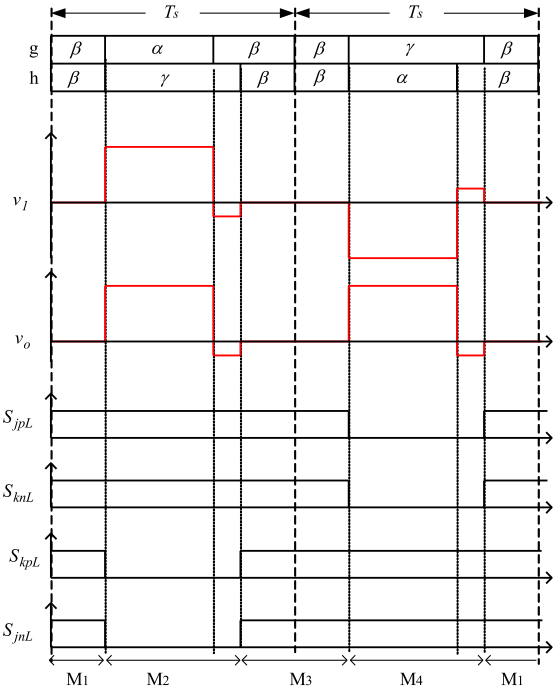

FIGURE 7. Switching pattern of the DC-AC H-bridge converter.

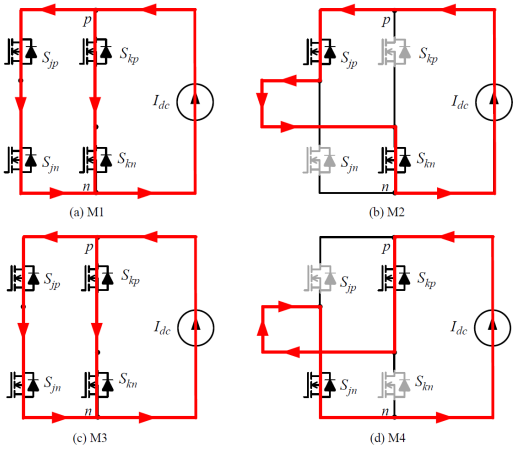

FIGURE 8. Current directions in the DC-AC H-bridge converter.

operations exist (M1-M4). As can be observed, the switching actions of the OFF-going switches of the HBC (S_{kp} & S_{jn}) at the end of Mode-1 and (S_{jp}& S_{kn}) at the end of Mode-3 are done before switching action of the MC enabling zero-voltage switching (ZVS). Also, switching actions of the ON-coming

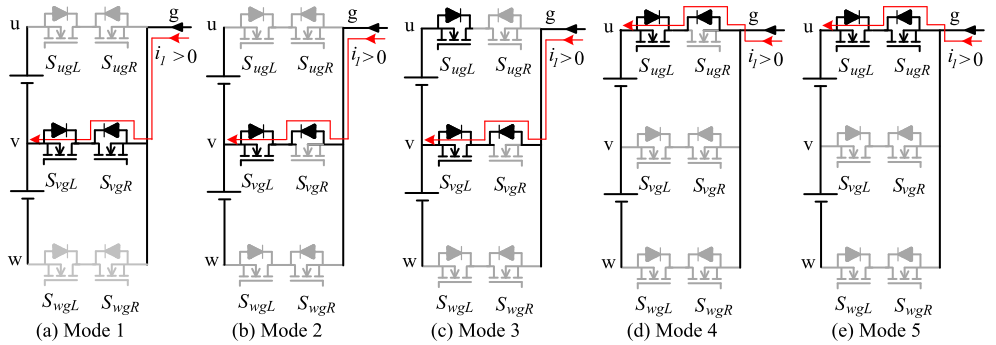

(I) Current transition from middle phase voltage (phase v) to maximum one (phase u)

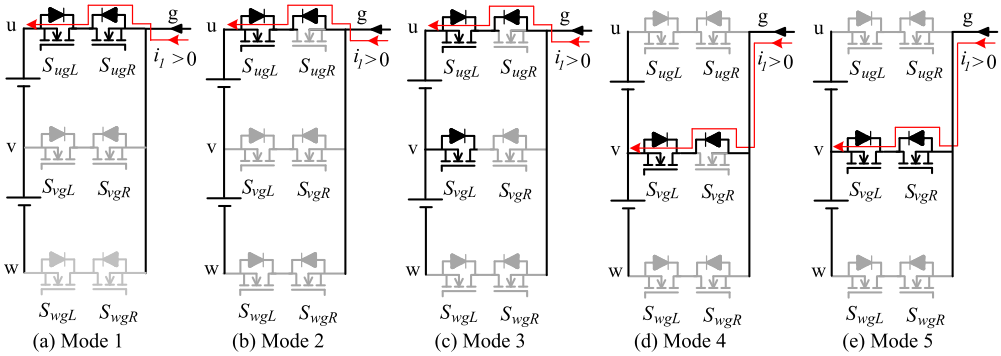

(II) Current transition from Maximum phase voltage (phase u) to maximum one (phase v)

FIGURE 9. Four-step commutation of matrix converter switches at the terminal (g).

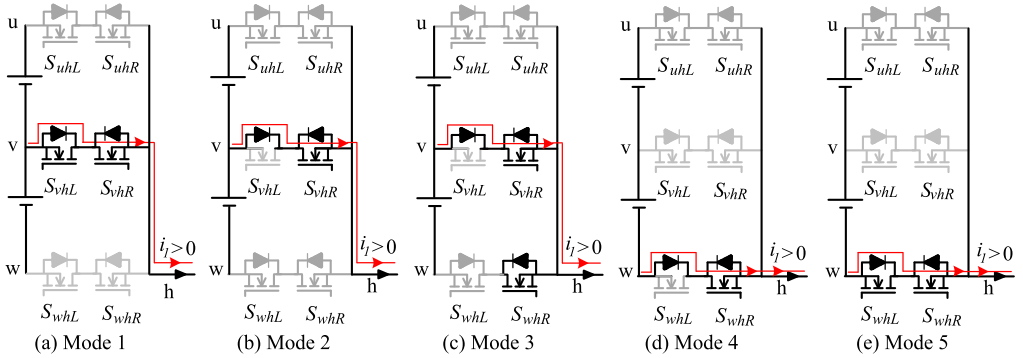

(I) Current transition from middle phase voltage (phase v) to a minimum one (phase w).

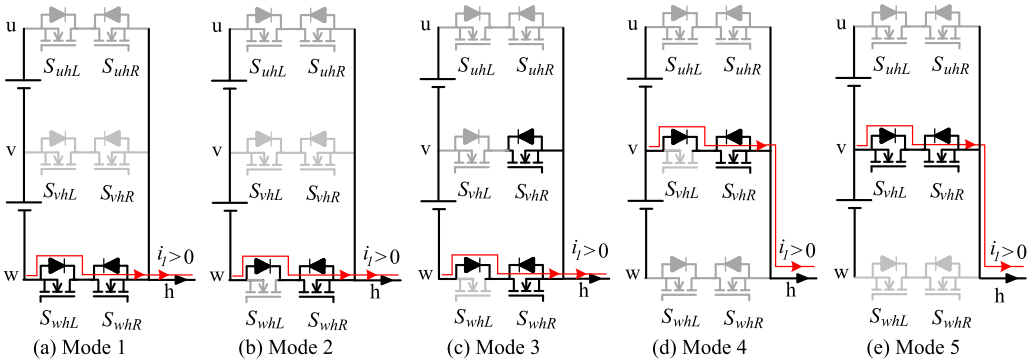

(II) Current transition from minimum phase voltage (phase w) to middle one (phase v)

FIGURE 10. Four-step commutation of matrix converter switches at the terminal (h).

switches of the HBC (S_{kp} & S_{jn}) at the end of Mode-2 and (S_{jp} & S_{kn}) at the end of Mode-4 are done after switching action of the matrix converter enabling ZVS.

On the other hand, four-step commutation has been considered for smooth current transition between MC bidirectional switches. Fig. 9 shows the current transition between

bidirectional switches of middle and maximum phase voltage levels connecting terminal (g) with the three-phase grid side. On the other hand, Fig. 10 shows the current transition between bidirectional switches of middle and minimum phase voltage levels connecting terminal (h) with the three-phase grid side.

VII. PWM SWITCHING TECHNIQUE OF H-BRIDGE AND MATRIX CONVERTER

Fig. 11 shows the PWM switching technique of the H-bridge and matrix converter. All switching signals of matrix converter bidirectional switches are generated from the comparison between triangle carrier waveform and three modulation signals (C_{ma}, C_{mb}, and C_{mc}), calculated based on the duty cycle of the matrix converter in (12) and (13) for the positive and negative half-cycles, respectively. Modulation signals of the matrix converter can be formulated as follows:

$$\begin{cases} C_{mc} = \begin{cases} \dfrac{d_{\beta g}}{2} & if\ d_{\beta g} \le d_{\beta h} \\ \dfrac{d_{\beta h}}{2} & if\ d_{\beta g} > d_{\beta h} \end{cases} \\ C_{mb} = C_{mc} + d_{\alpha g} \\ C_{ma} = 1 - C_{mc} \end{cases} \tag{19}$$

On the other hand, all switching signals of HBC switches are generated from the comparison between triangle carrier waveform and two modulation signals (C_{sh} and C_{sl}), which are the same as modulation signals (C_{ma} and C_{mc}) with a small offset to realize a one-microsecond dead-time (T_{com}) between switching actions of HBC and matrix converter, hence confirming ZVS of all HBC switches. Modulation signals of HBC can be formulated as follows:

$$\begin{cases} C_{sh} = C_{ma} + \dfrac{T_{com}}{T_s} \\ C_{sl} = C_{mc} - \dfrac{T_{com}}{T_s} \end{cases} \tag{20}$$

A simple logic circuit, shown in Fig. 12, is used to generate gate signals of bidirectional switches connecting three-phase grid voltage terminals with matrix converter output upper terminal (g). Also, Fig. 13 shows a simple logic circuit used to generate gate signals of all HBC switches. The generated output signal (S_0) of the logic circuit shown in Fig. 13 is used to derive switches (S_{jp} and S_{kn}), whereas output signal (S_1) is used to derive switches (S_{jn} and S_{kp}).

VIII. PROPOSED CONTROL TECHNIQUE

Fig. 14 shows the block diagram of the proposed controller of the isolated grid-connected dc-ac-ac converter. In this technique, the actual dc-current is regulated to follow the

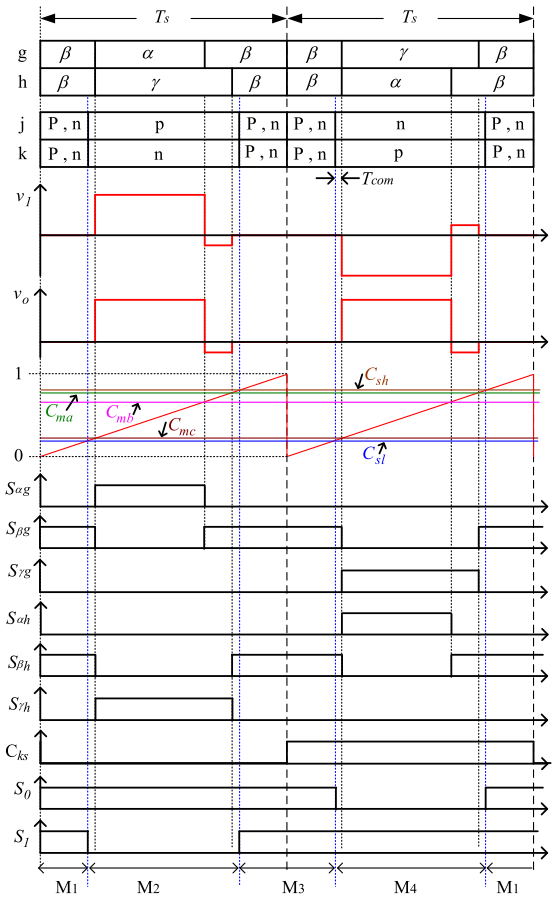

FIGURE 11. PWM switching technique of H-bridge and matrix converter.

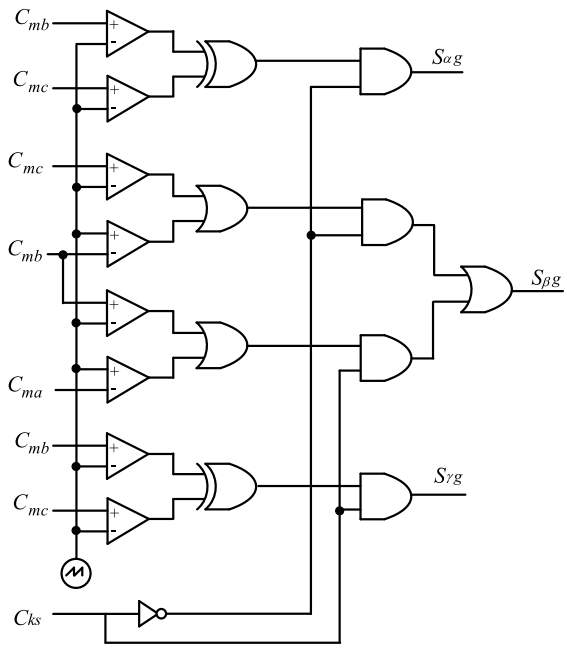

FIGURE 12. Logic circuit for generating MC gating pulses.

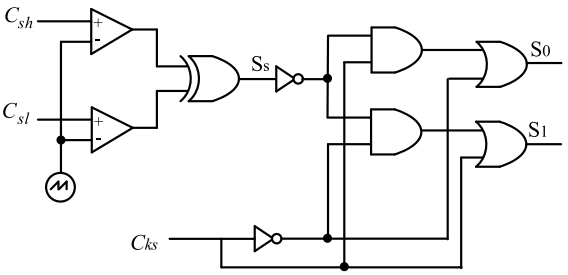

FIGURE 13. Logic circuit for generating HBC gating pulses.

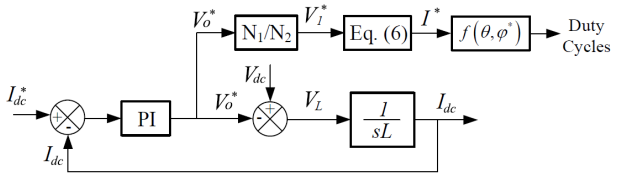

FIGURE 14. Control block diagram of the DC-AC-AC converter.

reference value via the PI-controller, as shown in Fig. 14. The output of the PI controller is considered as the reference of input voltage of the HBC, V_o^*. The transformer output voltage, V_1 can be obtained by considering its turns ratio, as shown in Fig. 14. The MC switching duties can be obtained according to the reference grid currents for the positive and negative half-cycles of the HF voltage waveform, respectively.

IX. EXPERIMENTAL RESULTS

Fig. 15 shows the proposed grid-connected isolated dc-ac-ac converter configuration. The experimental system parameters are listed in Table 1, while Fig. 16 shows the photographs of the converter prototype. In this system, the battery stored energy can be injected into the grid through a conventional H-bridge and the MC linked by a single-phase HFT. The conventional LC filter is used on the grid side to suppress the grid injected AC current's high-frequency components. The HFT has a 1:1 turn ratio. The experimental results are carried out based on the reference dc-current of 8 A and 4 A, enabling power flow of 1.6 kW and 0.8 kW, respectively, from the battery dc-side to the grid ac-side. Fig. 17 and Fig. 18 show the experimental results in the case of reference dc-current of 8 A and 4 A, respectively.

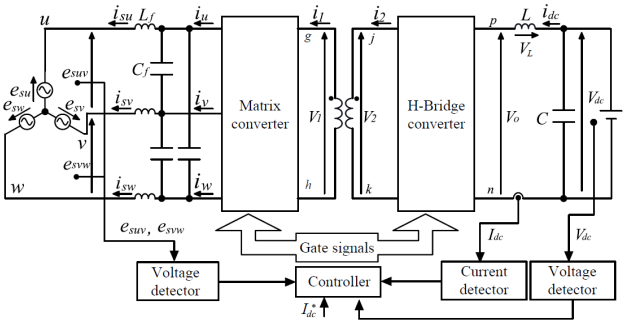

FIGURE 15. System configuration.

TABLE 1. Experimental System Parameters.

Parameter	Value
Source voltage, E, and ω	200 V and 377 rad/s
Battery DC voltage, V_{dc}	200 V
DC current reference, I_{dc}	8 A and 4 A
Inductance, L and Capacitance, C	4 mH and 1500 µF
Input filter, L_f and C_f	1.2 mH and 8.2 µF
Carrier frequency, f_s	20 kHz
The ratio of HF transformer, $N1:N2$	1:1

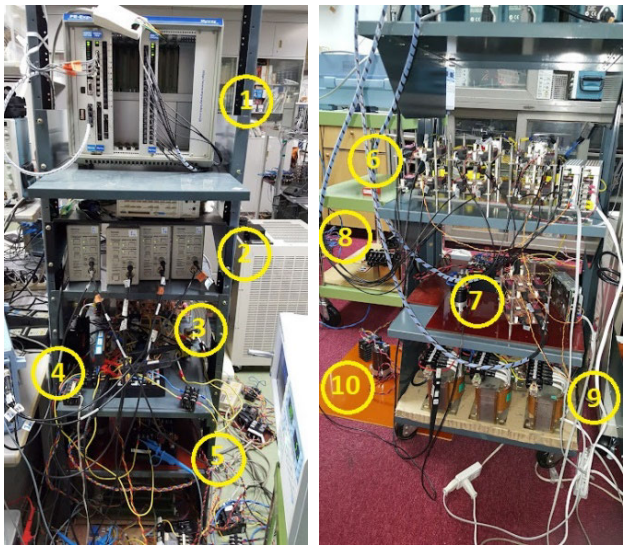

(a) Front side (b) Back-side

① Expert-III controller, ② Current measurements, ③ High-frequency transformer, ④ Matrix converter, ⑤ H-bridge converter, ⑥ Gate driver of matrix converter, ⑦ Gate driver of H-bridge converter, ⑧ DC side filter, ⑨ Grid side filter, and ⑩ DC supply.

FIGURE 16. Photograph of Experimental Prototype.

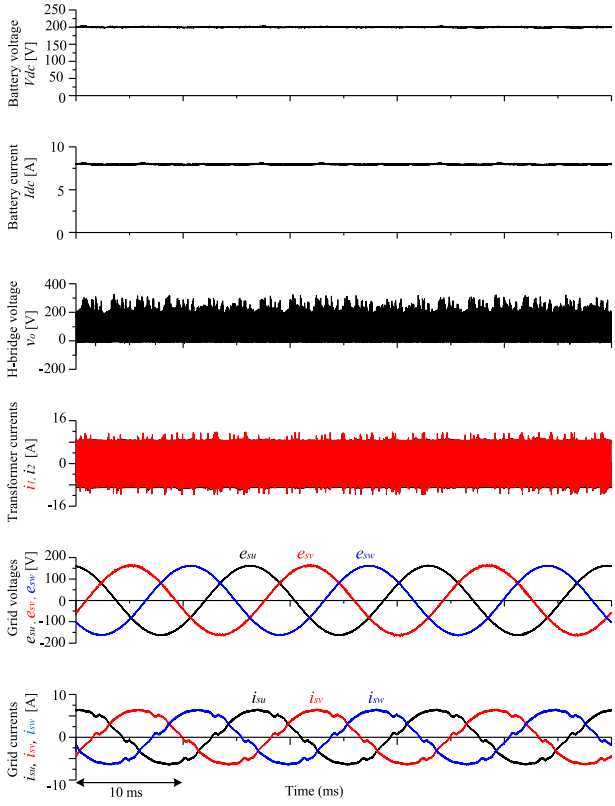

FIGURE 17. Experimental results in the case of 1.6kW power flow.

The battery dc voltage V_{dc}, battery dc-current, I_{dc}, H-bridge input voltage V_o, transformer input and output currents i_1; i_2, three-phase grid voltages v_{su}, v_{sv}, v_{sw} and

TABLE 2. Comparisons with Other Systems.

	References [14], [15]	Proposed
Control Approach	The power flow is controlled by adjusting the phase shift angle between primary and secondary voltages of HFT using an additional series inductor at HFT sides.	The power flow is controlled by adjusting the switching patterns and duty cycles of both matrix converter and HBC, hence no need for series inductors on the HFT side.
Control Objectives	• Controlling the phase shift angle between primary and secondary voltages of the single-phase HFT. • Controlling the input DC current. • Injecting sinusoidal currents to the grid at unity power factor.	• Controlling the power flow by adopting switching patterns and duty cycles of both converter stages. • Controlling the input DC current. • Injecting sinusoidal currents to the grid at unity power factor.
Merits	• Natural soft switching of HBC due to the lagging continuous current of HFT. • High efficiency due to the Continuous current in HFT.	• Natural soft-switching of HBC due to dead-time between switching of HBC and matrix converter • A simple control algorithm reduces execution time in the DSP system. • No additional series inductors at HFT sides reduces system footprint and cost. • Accurate duty cycles of matrix converter due to independence on system parameters • Low THD of the grid current
Demerits	• Additional series inductors at HFT sides increase system footprint and cost. • Phase shift angle between primary and secondary voltages of HFT depends mainly on the additional series inductors that may vary due to temperature or operating conditions resulting in inaccurate power flow control. • Modulation of the HFT current as a square waveform to simplify duty cycles calculations increases errors of the matrix converter duty cycles resulting in high THD at the grid current.	• The discontinuous current of the HFT slightly reduces system efficiency.

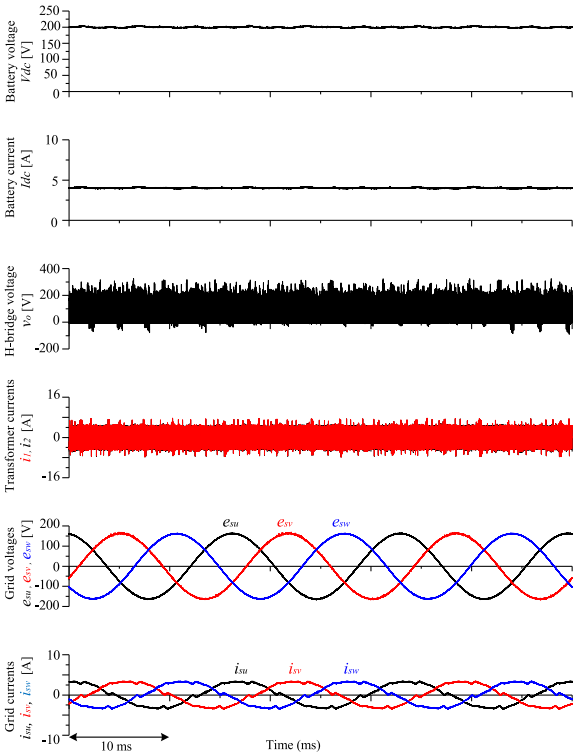

FIGURE 18. Experimental results in the case of 0.8kW power flow.

three-phase grid injected currents i_{su}, i_{sv}, i_{sw} are shown in Figs. 17 and 18. Both figures clearly show that the battery dc-current matches the reference values of 8 A in Fig. 17 and 4 A in Fig. 18. For a better presentation, zoomed waveforms of these results are shown in Fig. 19. Also, it can be observed that the grid injected current is a three-phase sinusoidal waveform with a unity power factor. However, the LC filter at the grid side slightly shifted the injected current from the grid voltage due to the capacitor leading current.

Fig. 20 shows the FFT harmonic spectrum of the grid injected currents waveform compared to the European IEC 61000-standard of the grid-tied converters in the range of 10 kW. Some distortions in the grid currents are observed from the experimental results of Figs. 17 and 18. However, their effects on the FFT spectrum are not significant, and the low-order harmonic components of the grid injected current is less than the permissible limits of the IEC standard, as shown in the FFT spectrum of Fig. 20. These distortions are owed to the proposed control and PWM switching techniques. Therefore, it was confirming the validity of the system for grid-tied applications. Moreover, Fig. 21 shows the efficiency profile of the system.

A similar topology of the proposed system was presented in [14], [15]. However, in [14], [15], the power flow was controlled by adjusting the phase shift angle between primary and secondary voltages of HFT. Therefore, the HFT leakage inductance was increased by adding extra series inductors at the primary and secondary sides leading to lagging continuous current flow in the HFT, hence natural soft-switching of all HBC switches. Also, the

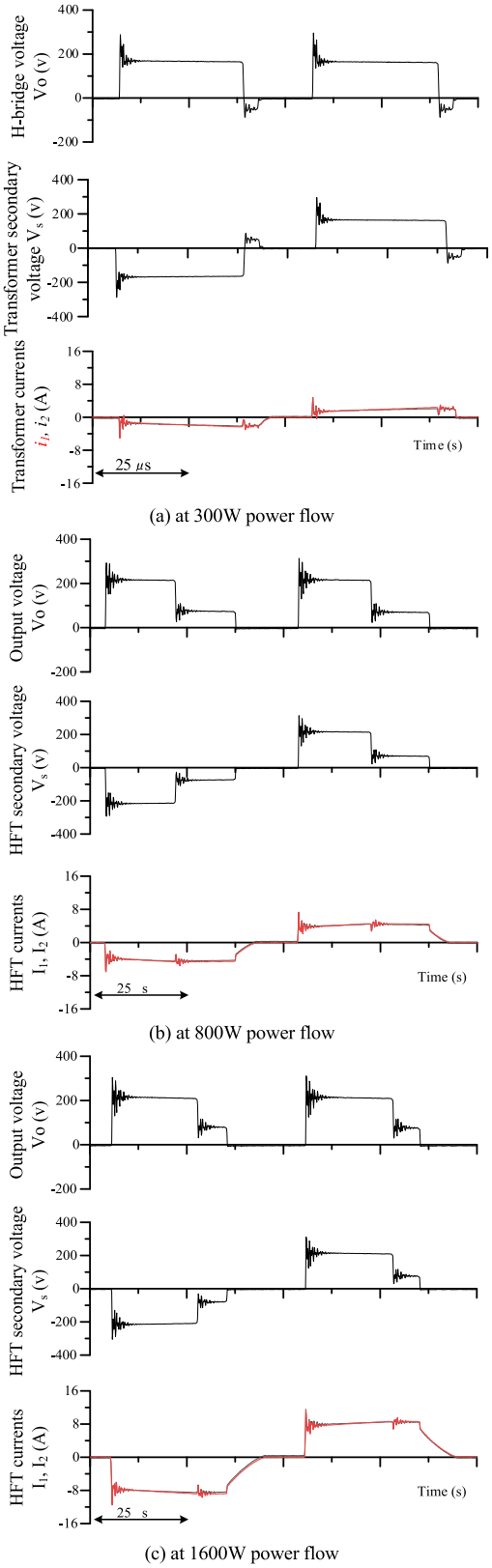

FIGURE 19. Zoomed waveforms of H-bridge output voltage, HFT secondary voltage, HFT currents for 300W, 800W, and 1600W.

continuous current flow in HFT increased system efficiency. However, the mathematical model presented in [14], [15]

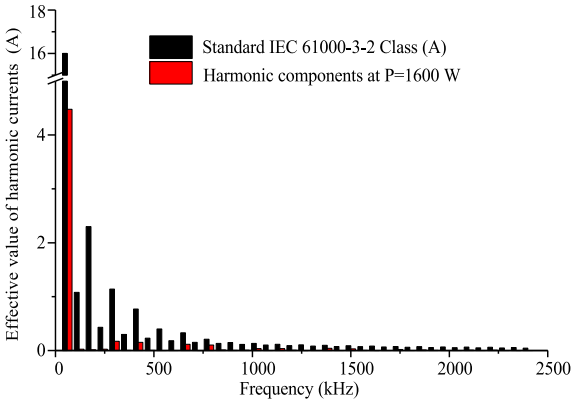

FIGURE 20. Low order harmonics of the grid current.

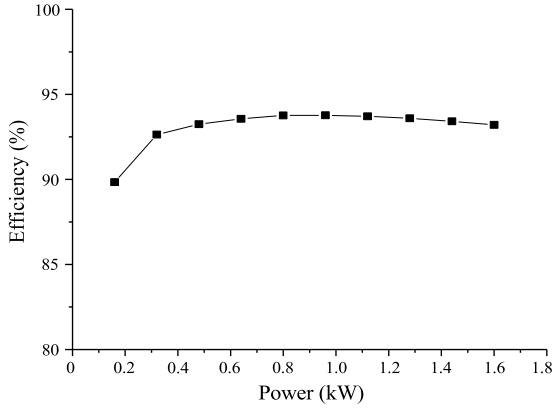

FIGURE 21. Efficiency profile of the system.

used a square-wave approximation of the HFT current that increases THD at the grid current. Also, the additional series inductors at HFT sides increase system footprint and cost.

On the other hand, the proposed topology in this paper does not utilize any additional inductors that increase power density and reduce cost. Also, the control technique is independent of the system parameters. Therefore, power flow is controlled by adopting switching patterns at both stages of the converter based on the calculated duty cycles, which in turn provides MC with accurate duty cycles, hence injecting sinusoidal current to the grid with lower THD. However, the discontinuous current in HFT slightly reduces system efficiency. Table 2 shows the comparison between the two systems.

X. CONCLUSION

This paper has presented a new and straightforward PWM switching technique for the isolated grid-connected three-phase dc-ac converter along with its mathematical modeling. The dc-ac converter has been designed to connect dc-battery to the utility grid through an HBC and a matrix converter linked by a single-phase high-frequency transformer (HFT). The HFT provides galvanic isolation between the battery and

grid sides. A simple modulation and control technique of the analyzed converter is proposed in this paper. Based on the proposed technique, the maximum voltage transfer ratio of the converter can be achieved, and a full battery dc-current control is also provided. An experimental test rig is developed to justify the proposed technique. Near sinusoidal injected grid current waveforms with acceptable low-order harmonic components, which are less than the permissible limits of the IEC standard, are obtained experimentally with a unity power factor. It is worth noting that the analyzed system with the proposed modulation and control technique has a small footprint, low cost, and high efficiency (about 93% as in the case study). These features make this system particularly valuable in integrating the BES with RES in the future power grid.

ACKNOWLEDGMENT

This publication was made possible by research collaboration between South Valley University, Nagoya Institute of Technology, Qatar University, and Jazan University. The statements made herein are solely the responsibility of the authors. The Open Access funding is provided by the South Valley University, Qena, Egypt.

REFERENCES

[1] J. Hong, J. Yin, Y. Liu, J. Peng, and H. Jiang, "Energy management and control strategy of photovoltaic/battery hybrid distributed power generation systems with an integrated three-port power converter," *IEEE Access*, vol. 7, pp. 82838–82847, 2019.

[2] S. Mortazavian and Y. A.-R.-I. Mohamed, "Investigation and enhancement of stability in grid-connected converter-based distributed generation units with dynamic loads," *IEEE Access*, vol. 8, pp. 93426–93443, 2020.

[3] W. Kang, M. Chen, B. Li, F. Chen, W. Lai, H. Lin, and B. Zhao, "Distributed reactive power control and SOC sharing method for battery energy storage system in microgrids," *IEEE Access*, vol. 7, pp. 60707–60720, 2019.

[4] F. M. Ibanez, "Bidirectional series resonant DC/AC converter for energy storage systems," *IEEE Trans. Power Electron.*, vol. 34, no. 4, pp. 3429–3444, Apr. 2019.

[5] B. Singh, B. N. Singh, A. Chandra, K. Al-Haddad, A. Pandey, and D. P. Kothari, "A review of three-phase improved power quality AC-DC converters," *IEEE Trans. Ind. Electron.*, vol. 51, no. 3, pp. 641–660, Jun. 2004.

[6] S. Hosseini, F. Sedaghati, and M. Sarhangzadeh, "Improved power quality three phase AC-DC converter," in *Proc. Int. Conf. Electr. Mach. Syst. (ICEMS)*, Oct. 2010, pp. 148–153.

[7] V. Fernão Pires, E. Romero-Cadaval, D. Vinnikov, I. Roasto, and J. F. Martins, "Power converter interfaces for electrochemical energy storage systems—A review," *Energy Convers. Manage.*, vol. 86, pp. 453–475, Oct. 2014.

[8] M. A. Hannan, P. J. Ker, M. S. H. Lipu, Z. H. Choi, M. S. A. Rahman, K. M. Muttaqi, and F. Blaabjerg, "State of the art of solid-state transformers: Advanced topologies, implementation issues, recent progress and improvements," *IEEE Access*, vol. 8, pp. 19113–19132, 2020.

[9] S. Baek and S. Bhattacharya, "Isolation transformer for 3-port 3-phase dual-active bridge converters in medium voltage level," *IEEE Access*, vol. 7, pp. 19678–19687, 2019.

[10] Y. Li, Q. Sun, D. Qin, K. Cheng, and Z. Li, "Power control of a modular three-port solid-state transformer with three-phase unbalance regulation capabilities," *IEEE Access*, vol. 8, pp. 72859–72869, 2020.

[11] D. Das, N. Weise, K. Basu, R. Baranwal, and N. Mohan, "A bidirectional soft-switched DAB-based single-stage three-phase AC–DC converter for V2G application," *IEEE Trans. Transport. Electrific.*, vol. 5, no. 1, pp. 186–199, Mar. 2019.

[12] H. V. Nguyen, D.-D. To, and D.-C. Lee, "Onboard battery chargers for plug-in electric vehicles with dual functional circuit for low-voltage battery charging and active power decoupling," *IEEE Access*, vol. 6, pp. 70212–70222, 2018.

[13] M. Amirabadi, J. Baek, and H. A. Toliyat, "Bidirectional soft-switching series AC-link inverter," *IEEE Trans. Ind. Appl.*, vol. 51, no. 3, pp. 2312–2320, May/Jun. 2015.

[14] M. A. Sayed, K. Suzuki, T. Takeshita, and W. Kitagawa, "PWM switching technique for three-phase bidirectional grid-tie DC–AC–AC converter with high-frequency isolation," *IEEE Trans. Power Electron.*, vol. 33, no. 1, pp. 845–858, Jan. 2018.

[15] M. A. Sayed, K. Suzuki, T. Takeshita, and W. Kitagawa, "Soft-switching PWM technique for grid-tie isolated bidirectional DC–AC converter with SiC device," *IEEE Trans. Ind. Appl.*, vol. 53, no. 6, pp. 5602–5614, Nov. 2017.

[16] M. A. Sayed, T. Takeshita, and W. Kitagawa, "Advanced PWM switching technique for accurate unity power factor of bidirectional three-phase grid-tied DC–AC converters," *IEEE Trans. Ind. Appl.*, vol. 55, no. 6, pp. 7614–7627, Nov. 2019.

[17] A. Garcés and M. Molinas, "A study of efficiency in a reduced matrix converter for offshore wind farms," *IEEE Trans. Ind. Electron.*, vol. 59, no. 1, pp. 184–193, Jan. 2012.

[18] R. Barrera-Cardenas and M. Molinas, "Comparative study of wind turbine power converters based on medium-frequency AC-link for offshore DC-grids," *IEEE J. Emerg. Sel. Topics Power Electron.*, vol. 3, no. 2, pp. 525–541, Jun. 2015.

[19] B. Veerasamy, W. Kitagawa, and T. Takeshita, "Input power factor control of bi-directional AC/DC converter," in *Proc. IEEE 10th Int. Conf. Power Electron. Drive Syst. (PEDS)*, Apr. 2013, pp. 1103–1108.

[20] Y. Fujishima, W. Kitagawa, and T. Takeshita, "Discharge operation of single-stage buck bi-directional AC/DC converter," in *Proc. 1st Int. Future Energy Electron. Conf. (IFEEC)*, Nov. 2013, pp. 12–17.

[21] J.-C. Kim, S. Kwak, and T. Kim, "Power factor control method based on virtual capacitors for three-phase matrix rectifiers," *IEEE Access*, vol. 7, pp. 12484–12494, 2019.

[22] J. C. Kim and S. Kwak, "Direct power control method with minimum reactive power reference for three-phase AC-to-DC matrix rectifiers using space vector modulation," *IEEE Access*, vol. 7, pp. 67515–67525, 2019.

[23] M. Yamada and T. Takeshita, "PWM strategy of AC to DC converter with high frequency link for reducing output voltage ripple," in *Proc. 4th Int. Conf. Power Eng., Energy Electr. Drives*, May 2013, pp. 846–851.

[24] K. Suzuki and T. Takeshita, "Input power factor control of high-frequency-link AC/DC converter," in *Proc. Int. Conf. Renew. Energy Res. Appl. (ICRERA)*, Oct. 2014, p. 815.

[25] N. Holtsmark, H. J. Bahirat, M. Molinas, B. A. Mork, and H. K. Hoidalen, "An all-DC offshore wind farm with series-connected turbines: An alternative to the classical parallel AC model?" *IEEE Trans. Ind. Electron.*, vol. 60, no. 6, pp. 2420–2428, Jun. 2013.

[26] K. Musasa, N. I. Nwulu, M. N. Gitau, and R. C. Bansal, "Review on DC collection grids for offshore wind farms with high-voltage DC transmission system," *IET Power Electron.*, vol. 10, no. 15, pp. 2104–2115, Dec. 2017.

[27] F. Fang, H. Tian, and Y. Li, "SVM strategy for mitigating low-order harmonics in isolated AC–DC matrix converter," *IEEE Trans. Power Electron.*, vol. 36, no. 1, pp. 583–596, Jan. 2021.

[28] S.-C. Ahn and D. S. Hyun, "New control scheme of three-phase PWM AC/DC converter without phase angle detection under the unbalanced input voltage conditions," *IEEE Trans. Power Electron.*, vol. 17, no. 5, pp. 616–622, Sep. 2002.

[29] W. Xiong, Y. Sun, J. Lin, M. Su, H. Dan, M. Rivera, and J. M. Guerrero, "A cost-effective and low-complexity predictive control for matrix converters under unbalanced grid voltage conditions," *IEEE Access*, vol. 7, pp. 43895–43905, 2019.

[30] S. Feng, J. Lei, J. Zhao, W. Chen, and F. Deng, "Improved reference generation of active and reactive power for matrix converter with model predictive control under input disturbances," *IEEE Access*, vol. 7, pp. 97001–97012, 2019.

[31] S. A. Q. Mohammed and J.-W. Jung, "A state-of-the-art review on soft-switching techniques for DC–DC, DC–AC, AC–DC, and AC–AC power converters," *IEEE Trans. Ind. Informat.*, vol. 17, no. 10, pp. 6569–6582, Oct. 2021.

MAHMOUD A. SAYED (Senior Member, IEEE) was born in Qena, Egypt, in 1974. He received the B.Sc. and M.Sc. degrees in electrical engineering from Minia University, Minia, Egypt, in 1997 and 2001, respectively, and the Ph.D. degree in electrical engineering from the Nagoya Institute of Technology, Nagoya, Japan, in 2010. Since 1999, he has been with the Department of Electrical Engineering, Faculty of Energy Engineering, Aswan University, Aswan, Egypt, first as an Administrator. Since 2001, he has been as a Lecturer. Since 2010, he has been with the Faculty of Engineering, South Valley University, Qena, first as an Assistant Professor, since 2015 as an Associate Professor, and currently as a Full Professor. His research interests include voltage regulation and loss minimization of electrical distribution systems using series and shunt power converters, pulse width modulation (PWM) techniques for bidirectional ac/dc and direct ac/ac converters, modular multilevel converters (MMxC), single and three-phase multilevel inverters, battery charger, power regeneration techniques for electric vehicles, in addition to renewable energy applications and machine drives. He is a Senior Member of the IEEE Power Electronics and Industry Application Societies.

TAKAHARU TAKESHITA (Senior Member, IEEE) was born in Aichi, Japan, in August 1959. He received the B.S. and M.S. degrees in electrical engineering from the Nagoya Institute of Technology, Nagoya, Japan, in 1982 and 1984, respectively, and the Ph.D. degree from Nagoya University, Nagoya, in 1990. Since 1991, he has been with the Nagoya Institute of Technology, where he is currently a Full Professor and is engaged in research on power converters and motor drives. He is a member of the Society of Instrument and Control Engineers (SICE) and Society of Signal Processing Applications and Technology of Japan (SSPATJ).

ATIF IQBAL (Senior Member, IEEE) received the B.Sc. (Hons.) and M.Sc. degrees in engineering (power system & drives) from Aligarh Muslim University (AMU), Aligarh, India, in 1991 and 1996, respectively, the Ph.D. degree from Liverpool John Moores University, Liverpool, U.K., in 2006, and the D.Sc. (Habilitation) degree in control, informatics, and electrical engineering from the Gdańsk University of Technology, Poland, in 2019. He is currently a Full Professor with the Department of Electrical Engineering, Qatar University, and a Former Full Professor with the Department of Electrical Engineering, AMU. He has been worked as a Lecturer with the Department of Electrical Engineering, AMU, since 1991, where he worked as a Full Professor, until August 2016. He has published widely in international journals and conferences his research findings related to power electronics, variable speed drives, and renewable energy sources. He has authored or coauthored more than 420 research papers and four books, and several chapters in edited books. He has supervised several large research and development projects worth more than multi-million USD. He has supervised and co-supervised several Ph.D. students. His research interests include smart grid, complex energy transition, active distribution networks, electric vehicles drivetrain, sustainable development and energy security, distributed energy generation, and multiphase motor drive systems. He is a fellow of IET (U.K.), fellow IE (India), and the Vice-Chair, IEEE Qatar Section. He was a recipient of Outstanding Faculty Merit Award academic, from 2014 to 2015, and the Research excellence awards at Qatar University, Doha, Qatar, in 2015 and 2019. He was also a recipient of the Maulana Tufail Ahmad Gold Medal for standing first at B.Sc.Eng. (electrical) Exams from AMU, in 1991. He has received several best research papers awards, e.g., at IEEE ICIT-2013, IET-SEISCON-2013, SIGMA 2018, IEEE CENCON2019, IEEE ICIOT 2020, and Springer ICRP 2020. He is also an Associate Editor of IEEE TRANSACTION ON INDUSTRIAL ELECTRONICS, IEEE ACCESS, the Editor-in-Chief of the *Journal of Electrical Engineering*, a Former Associate Editor of IEEE TRANSACTION ON INDUSTRY APPLICATION, and a Former Guest Associate Editor of IEEE TRANSACTION ON POWER ELECTRONICS.

ZUHAIR MUHAMMED ALAAS (Member, IEEE) received the B.S. degree from the King Fahad University of Petroleum and Minerals (KFUPM), Dhahran, Saudi Arabia, in 2002, the M.S. degree from the University of Newcastle upon Tyne, Newcastle, U.K., in 2007, and the Ph.D. degree from Wayne State University, Detroit, MI, USA, in 2017, all in electrical engineering. From September 2002 to November 2010, he worked as a Lecturer with the Abha College, Technical and Vocational Training Corporation, Saudi Arabia. From November 2010 to June 2011, he worked at Saudi Electric Company as a Power Transmission Engineer. Since June 2011, he has been joined Jazan University, where he is currently an Assistant Professor and the Department of Electrical Engineering Chairperson. His current research interests include energy storage devices, power electronics, microgrids, alternative/hybrid energy power generation systems, and motor drives.

M. M. R. AHMED (Member, IEEE) was born in Cairo, Egypt, in 1967. He received the B.E.E. degree from Helwan University, Helwan, Egypt, in 1989, the M.Sc. degree in electrical engineering from Cairo University, Cairo, in 1994, and the Ph.D. degree in electrical engineering from Northumbria University, Newcastle-upon-Tyne, U.K., in 2002. He was a Lecturer with the National Civil Aviation Training Institute, Cairo, from 1990 to 1991, followed by four years as an Administrate and a Teacher with the Industrial Education College, Cairo. From 1993 to 1996, he was a Teacher with the Abha Technical College, Abha, Saudi Arabia. He is currently a Lecturer with the Faculty of Industrial Education, Cairo. His research interests include power electronics, microcomputer control, DC motor drives, power systems, power quality, and applications of power electronics in power systems.

SHERIF M. DABOUR (Senior Member, IEEE) received the B.Sc. degree in electrical engineering from Zagazig University, Egypt, in 2002, and the M.Sc. and Ph.D. degrees in electrical power engineering from Tanta University, Egypt, in 2012 and 2015, respectively. From 2003 to 2009, he was a Certified Trainer at Technical and Vocational Training Corporation, Riyadh, Saudi Arabia. Since 2009, he has been joined the Faculty of Engineering, Tanta University, where he is currently an Associate Professor and a Coordinator of the Power Electronics Applications Research Laboratory. He is also serving as a Treasurer of the IEEE Power Electronics Society (PELS) Egypt Chapter. Moreover, he is also a Reviewer of several journals, including IEEE TRANSACTION ON POWER ELECTRONICS, IEEE TRANSACTION INDUSTRIAL ELECTRONICS, *IET Power Applications*, and *IET Power Electronics*. His research interests include PWM techniques, power converters, matrix converters, electric drives, and renewable energy conversion systems.